



3 4456 0278989 1

ORNL/TM-10562

oml

OAK RIDGE NATIONAL LABORATORY

MARTIN MARIETTA

Preliminary Creep and Pillar Closure Data for Shales

T. F. Lomenick
J. E. Russell

OAK RIDGE NATIONAL LABORATORY
 CENTRAL RESEARCH LIBRARY
 CIRCULATION SECTION
 ROOM 7000 115
LIBRARY LOAN COPY
 DO NOT TRANSFER TO ANOTHER PERSON
 If you wish someone else to see this
 report, send in name with report and
 the library will arrange a loan.

OPERATED BY
MARTIN MARIETTA ENERGY SYSTEMS, INC.
FOR THE UNITED STATES
DEPARTMENT OF ENERGY

Printed in the United States of America. Available from
National Technical Information Service
U.S. Department of Commerce
5285 Port Royal Road, Springfield, Virginia 22161
NTIS price codes—Printed Copy: A03; Microfiche A01

This report was prepared as an account of work sponsored by an agency of the United States Government. Neither the United States Government nor any agency thereof, nor any of their employees, makes any warranty, express or implied, or assumes any legal liability or responsibility for the accuracy, completeness, or usefulness of any information, apparatus, product, or process disclosed, or represents that its use would not infringe privately owned rights. Reference herein to any specific commercial product, process, or service by trade name, trademark, manufacturer, or otherwise, does not necessarily constitute or imply its endorsement, recommendation, or favoring by the United States Government or any agency thereof. The views and opinions of authors expressed herein do not necessarily state or reflect those of the United States Government or any agency thereof.

Chemical Technology Division
NUCLEAR AND CHEMICAL WASTE PROGRAMS
(Activity No. DB 02 04 02 0; ONWZ01D)

PRELIMINARY CREEP AND PILLAR CLOSURE DATA FOR SHALES

T. F. Lomenick and J. E. Russell*

*Texas A&M University, College Station, Texas.

Date of Issue — October 1987

NOTICE: This document contains information of a preliminary nature.
It is subject to revision or correction and therefore does not
represent a final report.

Research sponsored by the Office of Civilian Radioactive Waste
Management, U.S. Department of Energy

Prepared by the
OAK RIDGE NATIONAL LABORATORY
Oak Ridge, Tennessee 37831
operated by
MARTIN MARIETTA ENERGY SYSTEMS, INC.
for the
U.S. DEPARTMENT OF ENERGY
under contract DE-AC05-84OR21400



3 4456 0278989 1

CONTENTS

	<u>Page</u>
ABSTRACT.	1
1. INTRODUCTION	1
2. SUMMARY OF PREVIOUS WORK	2
3. DESCRIPTION OF TESTS	4
4. SIMULATION OF MINE PILLARS AND MODEL SCALING	8
5. TEST RESULTS	14
6. CONCLUSIONS.	28
7. REFERENCES	30

PRELIMINARY CREEP AND PILLAR CLOSURE DATA FOR SHALE ROCKS

T. F. Lomenick and J. E. Russell

ABSTRACT

The results of fourteen laboratory creep tests on model pillars of four different shales are reported. Initial pillar stresses range from 6.9 MPa (1000 psi) to 69 MPa (10,000 psi) and temperatures range from ambient to 100°C. Laboratory response data are used to evaluate the parameters in the transient power-law pillar closure equation similar to that previously used for model pillars of rock salt. The response of the model pillars of shale shows many of the same characteristics as for rock salt. Deformation is enhanced by higher stresses and temperatures, although the shale pillars are not as sensitive to either stress or temperature as are pillars of rock salt. These test results must be considered very preliminary since they represent the initial, or scoping, phase of a comprehensive model pillar test program that will lead to the development and validation of creep laws for clay-rich rocks.

1. INTRODUCTION

Because of its unique containment properties, shale is believed to be an extremely desirable host rock for the disposal of high-level radioactive wastes. The principal advantage of utilizing shale as a disposal medium for high-level wastes is its very low permeability to the flow of ground water. This property is due to its small sizes of matrix pores and its characteristic of deforming plastically at relatively shallow depths and/or low overburden loads (which promotes the self-healing of fractures). However, with emplacement of heat-generating wastes in shale strata unique mine stability problems may occur as a result of the elevated temperatures. To predict flow in the rocks, scale models of shale pillars and their surrounding rooms are being fabricated and tested from cores taken in four shales. These are believed to represent mineralogical extremes of shale types that may be suitable for repository utility.

The primary objective of this work is to provide data for the development and validation of creep laws for shales that are representative of strata that could be candidates for the disposal of

high-level radioactive wastes. In the future, these tests will be designed to systematically study the influence of (1) the material, (2) stress state, (3) temperature, (4) bedding plane orientation, and (5) the pillar shape (width/height ratio) on the time-dependent deformational response of the pillar. This report gives the results of a scoping study.

These results and future work on shales will provide data on the sensitivity of the mechanical response (pillar shortening) to increases in temperature and/or average pillar stress. That information will be useful during a national survey of shales when depth and lateral extent of various shale strata will be considered.

Although many shales may possess the geotechnical characteristics for containing and controlling emplaced wastes, our initial efforts are being directed toward four compositional end members, namely, the Devonian and Cambrian age deposits in the eastern United States and the Cretaceous and Cenozoic age sediments of the western United States. For this report, test data are reported for samples of the Huron shale of Devonian age, Conasauga Group (member unknown) of Cambrian age, the Pierre Shale of Cretaceous age, and the Green River Formation (oil shale) of Tertiary age. Composition and mechanical properties of three of the four shales considered here are given in Table 1, modified from Hansen and Vogt (1987).

2. SUMMARY OF PREVIOUS WORK

Analytical and numerical methods for simulating the behavior of rock pillars (required for stability) were not well developed in the early 1960's when laboratory work began on the concept of disposal of high-level radioactive waste in conventionally mined cavities in rocks. Consequently, a series of tests on physical models of mine pillars was initiated at Oak Ridge National Laboratory (ORNL). Obert (1964) had developed a laboratory-scale, model-pillar, constant-load creep test that accounted for the lateral confinement of the roof and floor rocks by steel bands. This test allowed for the study of the response of pillars with different width-to-height ratios and salt pillars with and without shale partings as described by Lomenick and

Table 1. Average composition and mechanical properties of shales^a

Mineral	Shale type ^b (wt %)		
	Green River	Conasauga	Pierre
Illite	3.9 ± 0.6	53.4 ± 3.4	3.5 to 13.6
Chlorite	0.0	20.4 ± 3.0	0.0 to 2.3
Kaolinite	0.0	0.0	1.9 to 8.7
Smectite	0.0	0.0	13.1 to 25.1
Nonclay/Detrital	31.3	24.0	14.6 to 32.9
Total carbonates (wt %)	50.5	0.0	56.5 - 19.1
Moisture content (wt %)	0.58	NA	18.4
Mechanical properties ^c :			
Ambient temperature:			
Co, MPa	94.8 ± 12.1	NA	7.2 ± 0.3
E (GPa)	10.4 ± 2.3	NA	0.6 ± 0.0
v	0.31 ± 0.1	NA	0.12 ± 0.02
150°C:			
Co, MPa	24.7 ± 2.5	NA	NA
E, GPa	0.8 ± 0.3	NA	NA
v	NA	NA	NA

^aUpper Huron Formation Shale data not available.

^bNumbers after ± are standard deviations. Data are from Hansen and Vogt (1987).

^cC₀ = unconfined compressive strength, E = Young's modulus, v = Poisson's ratio, NA = not available. 1 MPa = 145 psi, 1 GPa = 145,000 psi.

Bradshaw (1969a). Furthermore, the test could be run at elevated temperatures to simulate the conditions in a repository containing heat-generating nuclear waste.

Lomenick and Bradshaw (1969b) reported on an extensive testing program that included the effects of load, temperature, temperature elevation after initial loading, shale partings, pillar shapes, salt samples from different localities, reproducibility of results, ultimate strength, mechanisms of deformation, and long-term creep. That study resulted in the well known power-law pillar creep formula:

$$\epsilon = 1.30 \times 10^{-37} T^{9.5} \sigma^{3.0} t^{0.3} \quad (1)$$

where ϵ is the pillar shortening of a model pillar initially 25 mm (1 in.) high, T is absolute temperature (K), σ is the initial average pillar stress (psi) (1 MPa = 145 psi), and t is time in hours. Equation (1) holds for cylindrical model pillars with a width-to-height ratio of 4 fabricated from salt core from Lyons, Kansas.

Most of the test data used in developing Eq. (1) were obtained during tests of less than 1000 h duration. The longest testing time reported by Lomenick and Bradshaw (1969b) was slightly less than 30,000 h at room temperature and indicated that the deformation rate was still declining, which was consistent with observations in mine openings in the Lyons, Kansas salt mine. Longer term model pillar results have been analyzed by Russell and Lomenick (1984).

3. DESCRIPTION OF TESTS

To simulate pillar, roof, and floor conditions that would exist in mined cavities in shales, sample specimens in air-dry condition are fabricated to represent scale models of shale pillars and their surrounding rooms. The test specimens used in this work are cylindrical, with a portion of the center ground out to form the pillar and surrounding rooms. By "epoxying" steel rings around the ends of the samples, effective confining pressure is applied to the roof and floor portions of the models when they are loaded (see Fig. 1). Constant uniaxial loads are applied to the models by hydraulic

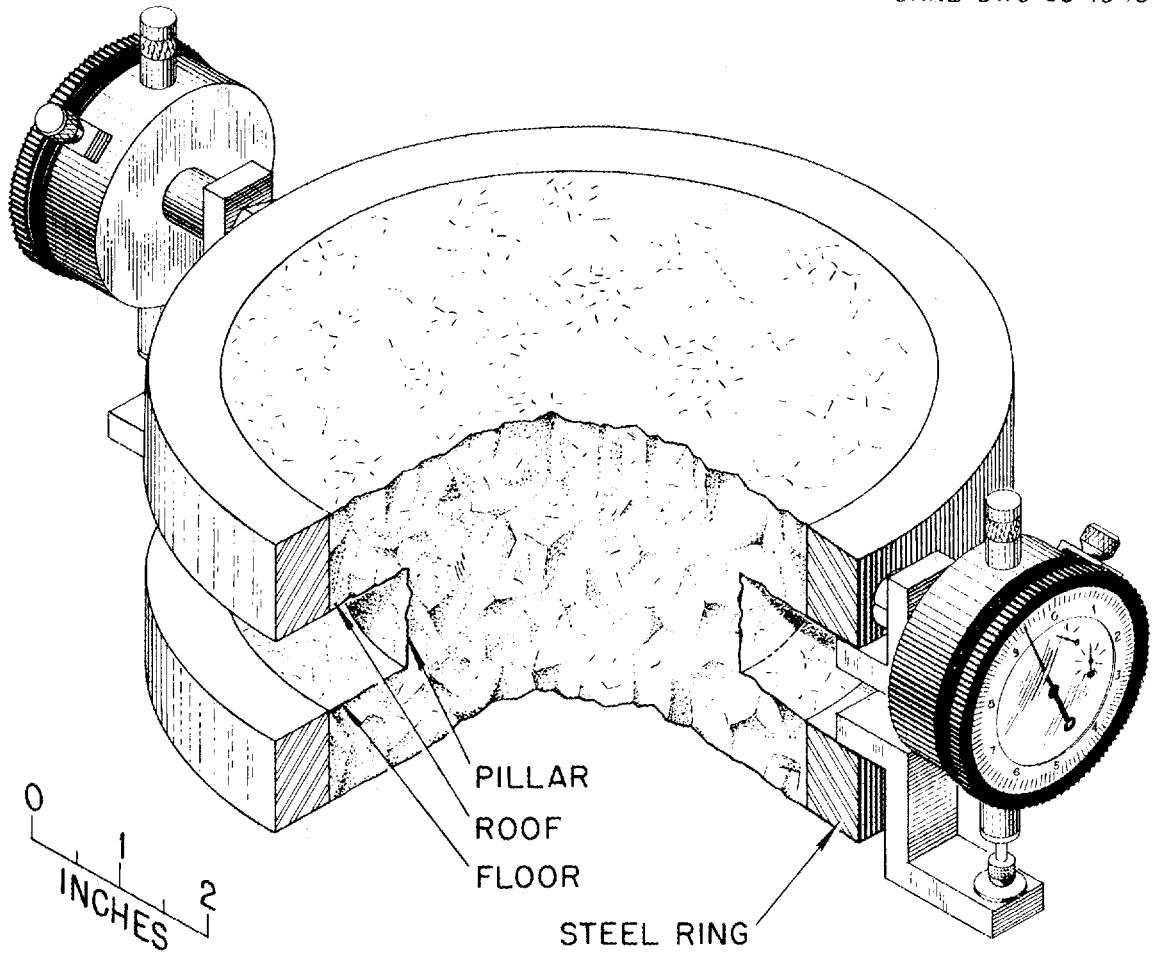


Fig. 1. Pillar model illustrating geometry, placements of steel rings, and displacement measuring gauges.

compression testers having capacities up to 1.3 MN (300,000 lbs). Cavity closure is measured by mounting two dial gauges 180° apart on the rings. Elevated temperature tests are performed with the specimens inside a cylindrical heating jacket and with barrier heaters on top and bottom between the specimen and the platens. No barriers are present to prevent moisture loss during the test.

The short-term tests reported here are performed on model pillars fabricated from cores of shale with dimensions given in Table 2. Refer to Table 3 for sample identification, depth, and test conditions. For model preparation, all cores were first cut to their approximate desired length by band saw and then finished by machine sanding. Next, steel confining rings (ASTM A-108, Grade 1018) were affixed to the tops and bottoms of the cores using Ciba Araldite 502 epoxy and Ciba hardener 951. For samples heated up to 100°C, Ciba Araldite 6005 epoxy and Pyrometallitic Dianhydride (PMDA) hardener are used. The unconfined center portion of the sample is then ground out, using a sanding disc attached to a standard drill press, to form the size pillar desired. Sheet teflon greased with a mixture of silicon grease and graphite is inserted between the tops and bottoms of the samples and the platens of the compression machines to reduce the friction between the rock and the platens to an insignificant amount. Chromel-Alumel thermocouples are emplaced in 1.5-mm (0.06-in.) diameter holes drilled into the center of the pillar, as well as at the outer edge to ensure a uniform temperature within the heated model specimens. A 12-point strip-chart recorder with a 0 to 350°C range is used to trace the temperature curves. A constant voltage transformer is used in supplying 118 volt AC to adjustable auto-transformers which are used as temperature controls for the cylindrical heating jackets, and the heaters in the platens at the top and bottom of the sample. In this manner, temperatures are regulated to within 1 to 2°C. In these scoping tests, no attempt has been made to determine the uniformity of temperature.

In general, the same test procedure is used for all specimens to ensure consistency. The procedure consists of rapidly applying a compressive load corresponding to 75% of the testing load and

Table 2. Specimen and pillar dimensions

Rock type	Specimen		Pillar		
	Diam.	Length	Width	Height	Width/Height
	(in.) (mm)	(in.) (mm)	(in.) (mm)	(in.) (mm)	
Green River Formation	6 (152)	5 (127)	4 (102)	1 (25)	4
Conasauga Formation	2.4 (61)	4.4 (112)	1.6 (41)	0.4 (10)	4
Pierre Shale	3.5 (89)	4.6 (117)	2.4 (61)	0.6 (15)	4
Huron Shale	3.5 (89)	4.6 (117)	2.4 (61)	0.6 (15)	4

Table 3. Model pillar test matrix

Rock type	Sample ID	Sample depth ft(m)	Av pillar stress MPa(psi)	Temp. (°C)	Start date	Duration (h)
Green River Formation	CR/86/	470(143)	28(4000)	22.5	1-13-86	1029
			42(6000)	22.5	3-3-86	1005
Conasauga Group	C/86/	725(221)	28(4000)	22.5	4-21-86	1055
			41(6000)	22.5	4-10-86	1055
			69 ^a (10,000)	22.5	5-28-86	1655
			28(4000)	100	5-12-86	2015
Pierre Shale	P/84/	216(66)	7(1000)	22.5	2-26-86	1010
			14(2000)	22.5	1-16-86	1010
			7(1000)	60	1-20-86	1012
Huron Shale	H/84/	515(157) 516(157) 523(159) 528(161)	28(4000)	22.5	6-20-85	4059
			41(6000)	22.5	7-8-85	4198
			69(10,000)	22.5	8-13-85	15,952
			42(6000)	100	7-10-85	2470
			28(4000)	100	3-18-86	1008

^aModel pillar data not used in empirical model development because of apparent material failure. All model pillars have a width-to-height ratio of 4.

releasing it, then applying a load of 85% of the test load which is also immediately released, and then applying 100% of the load. A base reading for the dial gauges is then taken. These initial loadings serve to seat the dial gauges, used to measure deformation, and to set the platens firmly on the sample. The deformation is recorded, first at intervals of seconds, then of minutes, and then at progressively longer intervals.

4. SIMULATION OF MINE PILLARS AND MODEL SCALING

The deformation characteristics of rock are extremely important considerations in the simulation of mine conditions in scale-model tests. To determine the stability of mine pillars composed of plastic materials like shale, it is absolutely necessary to simulate in the models, not only the mine pillar, but also the roof and floor conditions. The importance of the simulated roof and floor in the model pillars of shale can be illustrated by comparing test data from a model pillar with data obtained from testing a cylindrical specimen (without roof and floor constraint). In both cases, specimens were fabricated from 3.44-in.-diam (87.5 mm) cores of shale. For the model pillar specimens the center portion of the specimen was ground out to form the pillar [0.6-in. (15 mm) high x 2.4-in. diam (60 mm)] and the surrounding roof and floor. Steel rings were then "epoxied" to the top and bottom portion of the samples to restrain laterally the rock in the roof and floor (as would be the case in actual mine workings). On the other hand, for the specimens without roof and floor simulation, a cylindrical sample of shale having a diameter of 3.44 in. (87.5 mm) and a height of 0.6 in. (15 mm) (pillar only) was used for the test.

Pillar shortening data for the two specimens are given in Table 4. In both cases the rate of loading was 2.3 MPa (333 psi)/min. For shale samples tested at room temperatures, it was found that the model pillar specimen deformed nonlinearly with increasing stress; however, even after loading to 138 MPa (20,000 psi) the model continued to creep without catastrophic failure (pillar shortening reached about 30%). In comparison, the cylindrical specimen without roof and floor failed suddenly at 55 MPa (8000 psi). These data indicate that

actual mine conditions are simulated best when the roof and floor portions of the models are constrained laterally. This condition allows

Table 4. Comparison of shortening data for two specimens

Load (MPa) (psi)		Pillar shortening (%)	
		Model shale pillar with roof and floor	Shale pillar without roof and floor
14	2,000	0.03	0.3
28	4,000	0.32	3.1
41	6,000	0.6	8.5
55	8,000	1.4	Catastrophic failure
69	10,000	2.7	
83	12,000	8.9	
97	14,000	12.1	
110	16,000	16.5	
124	18,000	21.3	
138	20,000	29.6	

shear stress at the roof and floor to be transmitted into the pillar (at least for samples having a width-to-height ratio of 4), thereby increasing the mean stress in the pillar interior and decreasing the effective stress, which makes the pillar stronger.

Model pillar tests on rock salt were first presented by Obert (1964). The essential feature of these model pillars is the simulation of the role of the roof and floor material and stiffness in the axial creep of a pillar which is not accomplished by the common compression test. In the usual unconfined uniaxial compression test, an attempt is made to make the stress state as uniform as possible so that strength and/or deformation properties may be inferred as a function of stress. Such uniaxial tests are not designed to simulate mine pillars because they ignore roof-pillar and floor-pillar interactions. Length-to-diameter ratios normally range from 2 to 2.5 in order to isolate the center portion of the sample from end effects. These uniaxial tests do not, by themselves, simulate pillar behavior; but these data may be used in conjunction with confined triaxial test results to develop a constitutive model which can be used, with a computer code employing continuum mechanics principles, to simulate pillar behavior numerically. Model pillar data may be used as a first step in validation of the constitutive model and computer code.

In reviewing the model pillar tests and results, it should be kept clearly in mind that these are tests on models of a major structural component of the ground support system in a repository and are not materials tests per se. However, it is possible to infer parameters for creep laws from model pillar data as was done by Thoms (1973) and later by Wahi et al. (1977).

Another point to keep in mind about the model pillar tests is that they were originally designed for test durations of the order of months, not years. Furthermore, because of the inherent specimen-to-specimen variability in rocks, in a scoping study it is desirable to test many samples with less accuracy of measurement, rather than a few samples with greater accuracy, in order to capture the essential (first-order) changes in response caused by geometry, load, and temperature.

As with other types of structural modeling, the laws of similitude between the model and the prototype must be satisfied if the model is to exhibit the desired response. In reality, it is almost impossible to satisfy all the laws of similitude; and we are forced to attempt to simulate the desired response by maintaining similitude in the dominant variables. In this report, similitude is discussed as it relates to geometry, load, and temperature. For a more complete discussion of similitude as it relates to geology and structures in rock, the reader is referred to Obert and Duvall (1967) and Hubbert (1937).

A model is geometrically similar to a prototype if the ratios of all length dimensions in the model to the same model-to-length dimensions in the prototype are identical. If this is the case, all dimensions relative to a characteristic length in the model will be the same as in the prototype. In mine pillars, it is well known that the pillar width-to-height ratio is of primary importance; consequently, pillar height is chosen as the characteristic length. Salt mine pillars with width-to-height ratios less than unity have been known to fail in a brittle mode, while those with a ratio greater than 2 tend to flow rather than fracture (Obert and Duvall, 1967), although pillar spalling is observed if pillar shortening is large. Some shale pillars may exhibit similar behavior.

Lomenick and Bradshaw (1969a) reported on model pillar tests with width-to-height ratios from 2 to 4. All results presented herein are for a ratio of 4:1 which is representative of preliminary repository designs. Future work may consider other ratios and/or geometries.

As previously noted, one of the primary features of the model-pillar test is that it incorporates the influence of the roof and floor material and stiffness. In this case, the choice of a dimensionless ratio similar to the prototype is not as clear because the roof rocks extend to the surface and the floor rocks at least through the earth's crust. Thus, maintaining a similar ratio of depth to pillar height, for example, is realistically impossible. Lomenick (1969a) reports on a study of this question and concludes that maintaining a roof thickness-to-pillar height ratio of 2:1 is adequate to give reproducible results. The same ratio is maintained for the floor thickness-to-pillar height. This ratio is consistent with elasticity theory where one would expect the influence of stress concentrations caused by pillar-to-roof and floor intersections to be negligible a few characteristic lengths away.

The ratio of the annular width of the roof and floor to the pillar height has been maintained at ~1:1 for the tests reported here and, in this range, should not be a particularly significant parameter as far as pillar response is concerned; i.e., one would not expect much different pillar shortening response if this ratio were 1.3:1, provided that steel rings of adequate stiffness were provided. Note that these tests do not simulate roof and floor response. Lomenick and Bradshaw (1969a) measured the tangential strain in the steel roof rings in order to estimate the amount of confinement provided by these rings to the salt roof and floor. Similar measurements have not been made for model pillars of shale but are being considered for future tests.

The radius of curvature between the pillar vertical surface and the horizontal roof and floor surfaces has a significant effect on the elastic stress concentration in the immediate neighborhood of the intersection. The importance of this parameter has not been studied. If the radius is smaller for a particular model, plastic flow and stress redistribution will occur at lower values of vertical stress.

Of course, the average vertical pillar stress remains the same and is the parameter used in the empirical pillar creep law.

If actual mine pillars are considered, the pillar-to-roof or floor radius ratio depends on the excavation method and may be somewhat variable for mines using a drill-blast-load-haul system. This radius is much more uniform if a borer-type continuous miner is used. In this case, the radius may be approximately 0.3 m, and assuming two passes of the miner, the pillar height may be about 6 m leading to a radius-to-height ratio of $0.3:6 = 0.05$. For a model pillar 25 mm high, this would correspond to a radius of 1.25 mm. In the scoping study reported herein, no attempt is made to machine the specimens to a particular radius.

With respect to grain size, American Society for Testing and Materials (ASTM) standards for compression tests recommend a ratio of sample diameter to average grain size of 10 in order to provide a statistically representative cross section to help minimize sample-to-sample variability. Because of the dominance of clay size particles in shale rocks, this is not a matter of great concern for shales.

The most obvious geometric deviation of the model pillars from actual mine pillars is the circular horizontal cross-section of the model compared with the likely rectangular cross section of proposed repository pillars. The round models would probably simulate a square cross-section pillar better than a rectangular one with agreement becoming worse as the cross-section becomes more oblong. Bradshaw and McClain (1971) note that the pillar shape and size can probably be accounted for in the leading coefficient in the power law creep equation with the exponents remaining approximately the same as in the model pillars. Table 2 lists overall and model pillar geometries for each of the four shales considered here.

If a pillar near the center of a repository with lateral repository dimensions greater than the depth (i.e., wider than critical width) is considered, the average pillar stress can be estimated from the following tributary area equation:

$$\sigma_{av} = \gamma h / (1 - R), \quad (2)$$

where σ_{av} is the average pillar stress, γ is the weighted average specific weight of the overlying rocks, h is the depth from the

surface, and R is the areal extraction ratio (area removed/total area). Equation (2) holds regardless of temperature (assuming that it is also widely distributed and no arching can take place. The average pillar stress given by Eq. (2) is assumed to be that applied on the model pillar because the model material is the same as the prototype material. The total load applied to the model pillar is σ_{av} times the cross-sectional area of the model pillar. The total load simulates the weight of the rocks overlying the pillar and the area midway to the surrounding pillars. This total load remains constant during the life of the prototype and consequently is held constant during the pillar test even though the model pillar increases in diameter as it deforms and the actual average pillar stress decreases.

In view of the above considerations and subject to the assumptions made, the model pillar test maintains similitude with respect to load to the degree that the load is held constant over the duration of the test.

Similitude with respect to temperature is maintained to the degree that the temperature can be maintained uniform in time and space. In the case of the repository, the temperatures are not constant in either time or space. Spatial gradients will exist throughout the repository because of the heat production of the waste in the canisters to be placed in holes in the floor of the rooms. Temperature gradients will depend on design parameters such as (1) the thermal power per canister, (2) spacing and pitch of canisters, (3) room size, (4) pillar dimensions, and (5) heat conduction properties of the shale and overlying and underlying rocks. Temporal changes in temperature in a repository are expected because of the decaying nature of the thermal sources.

Heated-model pillar tests are not designed to simulate the exact response of a prototype pillar, but rather to provide information, such as the increase or decrease in pillar-shortening rate to be expected if the average pillar temperature is increased or decreased. Drying produces changes in thermal properties of shale which changes the time-dependent thermal response. Drying-induced changes in the transient thermal response are not exactly simulated by model pillars. Nevertheless, model pillar data are expected to be useful in validating the constitutive models and computer codes.

Salt mine pillars in areas of high extraction exhibit pillar slabbing or spalling. In such cases, the pillar may take on an approximate hour-glass shape formed by conjugate sets of shear fractures. Model pillars show similar tendencies, except that, in the case of salt, the material generally spalls off as individual grains. Lomenick and Bradshaw (1969a) presents photographs showing a salt model pillar and spalled material.

Another phenomena sometimes observed in mine pillars is punching; i.e., a stiff and strong pillar penetrates into a soft and weak floor and/or roof. Punching into the roof normally causes roof control problems which can sometimes be corrected by reducing the pillar size, and therefore stiffness, even though the extraction ratio may be held the same. The extent to which model pillars of salt punch into the simulated floor and roof is discussed by Lomenick and Bradshaw (1969a) who presented a photograph of the vertical cross-section of a previously tested model pillar showing this phenomena. Similar results are expected at least for the softer shales.

5. TEST RESULTS

Table 3 presents the shale model pillar test matrix for the model pillar geometries given in Table 2. Raw data from these tests were entered into a microcomputer for data reduction and analysis. Data reduction consisted of converting the dial gauge readings to incremental changes in pillar height and accumulating these changes. The cumulative displacements read from dial gauges 3 and 4 (gauges 1 and 2 are backup gauges) were averaged for each time and the average converted into nondimensional shortening by dividing by the initial pillar height, H, given in Table 2. Results for 13 of the 14 tests discussed are shown graphically in Figs. 2 to 9. Figures 2 to 9 indicate that most of the pillar creep response curves appear to have the form referred to as primary creep; i.e., the creep rate continues to slow down with time. Consequently, a transient creep response function of the form used for rock salt, Eq. (1), has been fitted to the shale data.

The empirical model chosen for preliminary analysis has the form

$$\epsilon = A \sigma^n T^u t^m \quad (3)$$

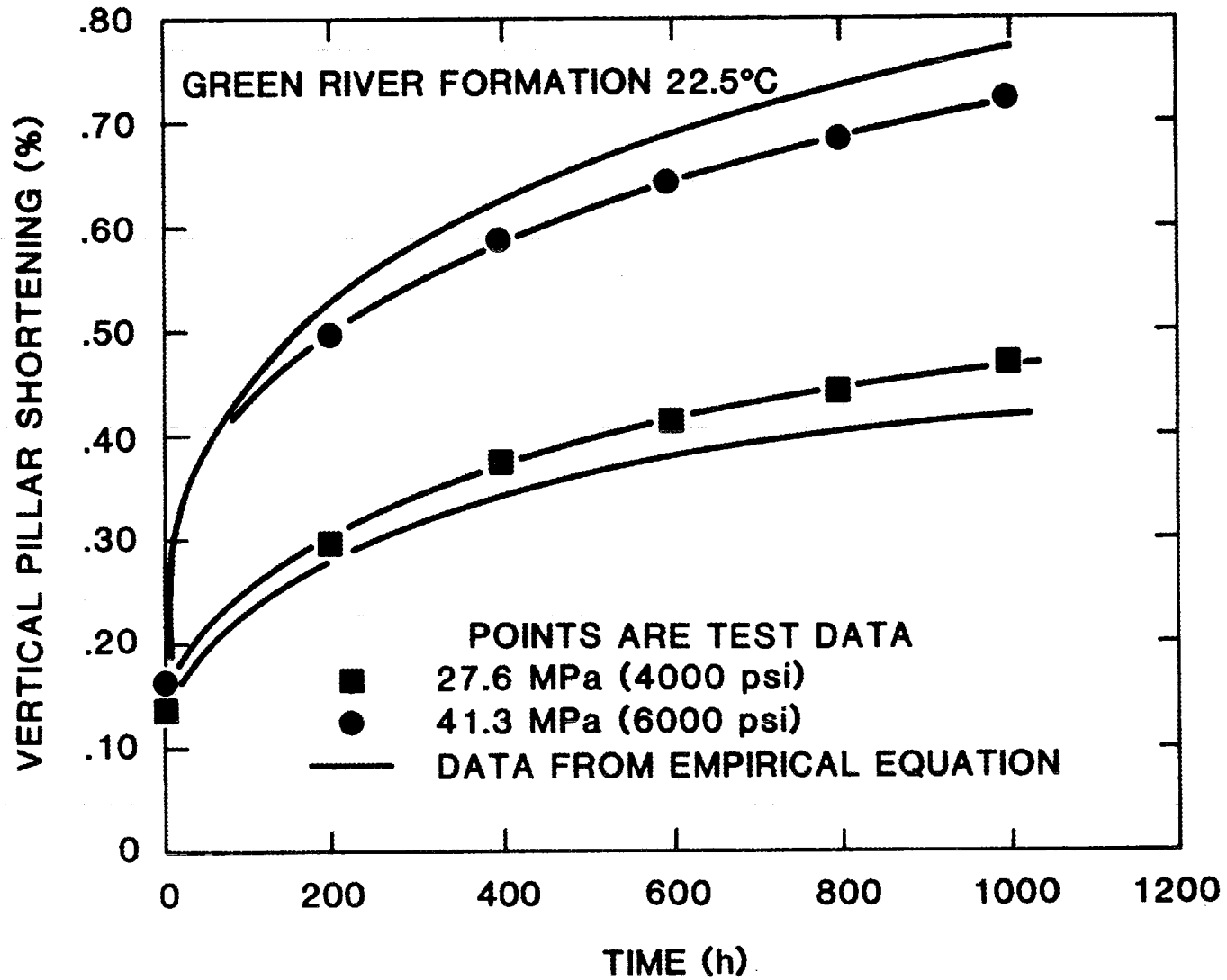


Fig. 2. Pillar shortening for Green River Formation at 22.5°C.

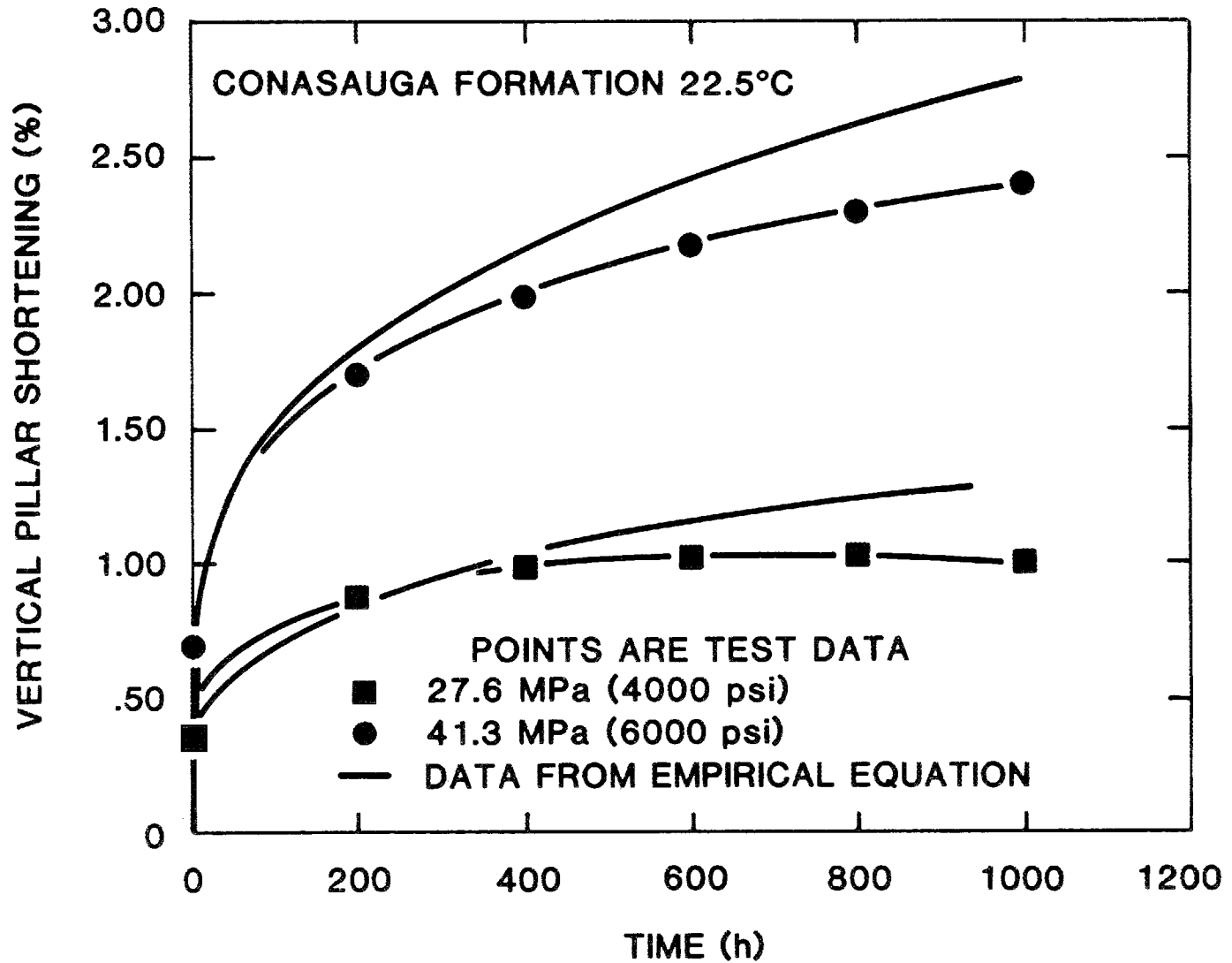


Fig. 3. Pillar shortening for Conasauga Formation at 22.5°C.

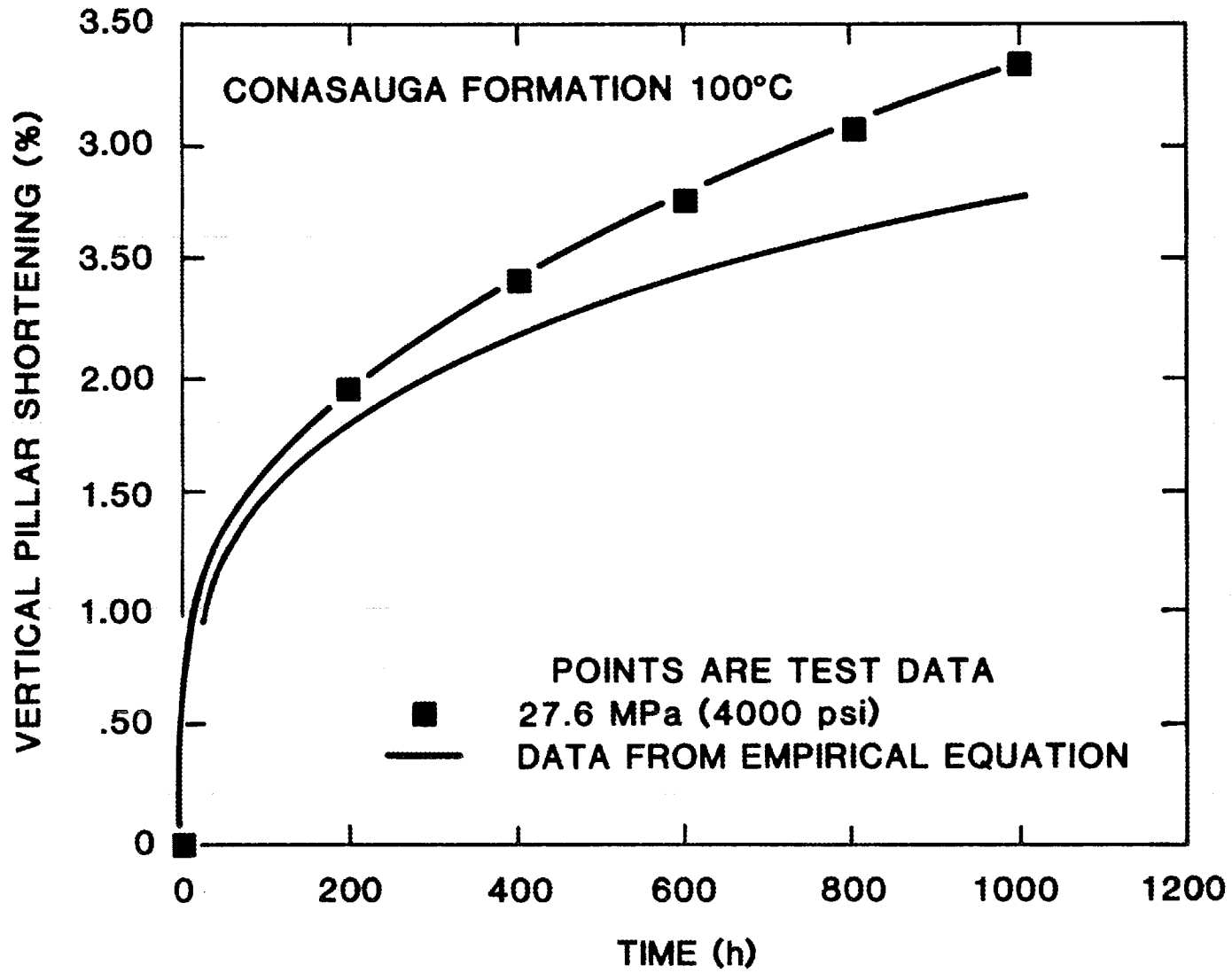


Fig. 4. Pillar shortening for Conasauga Formation at 100°C.

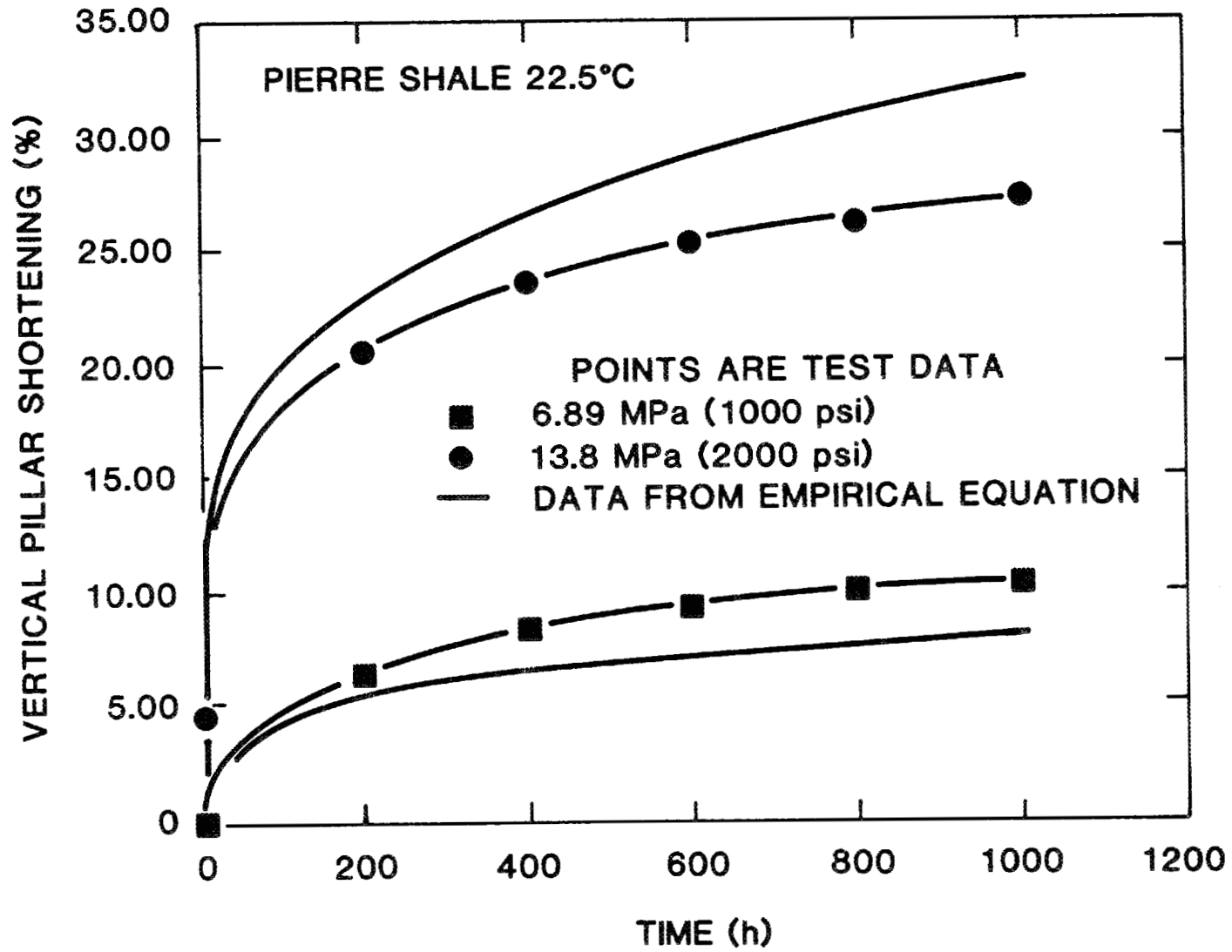


Fig. 5. Pillar shortening for Pierre Shale at 22.5°C.

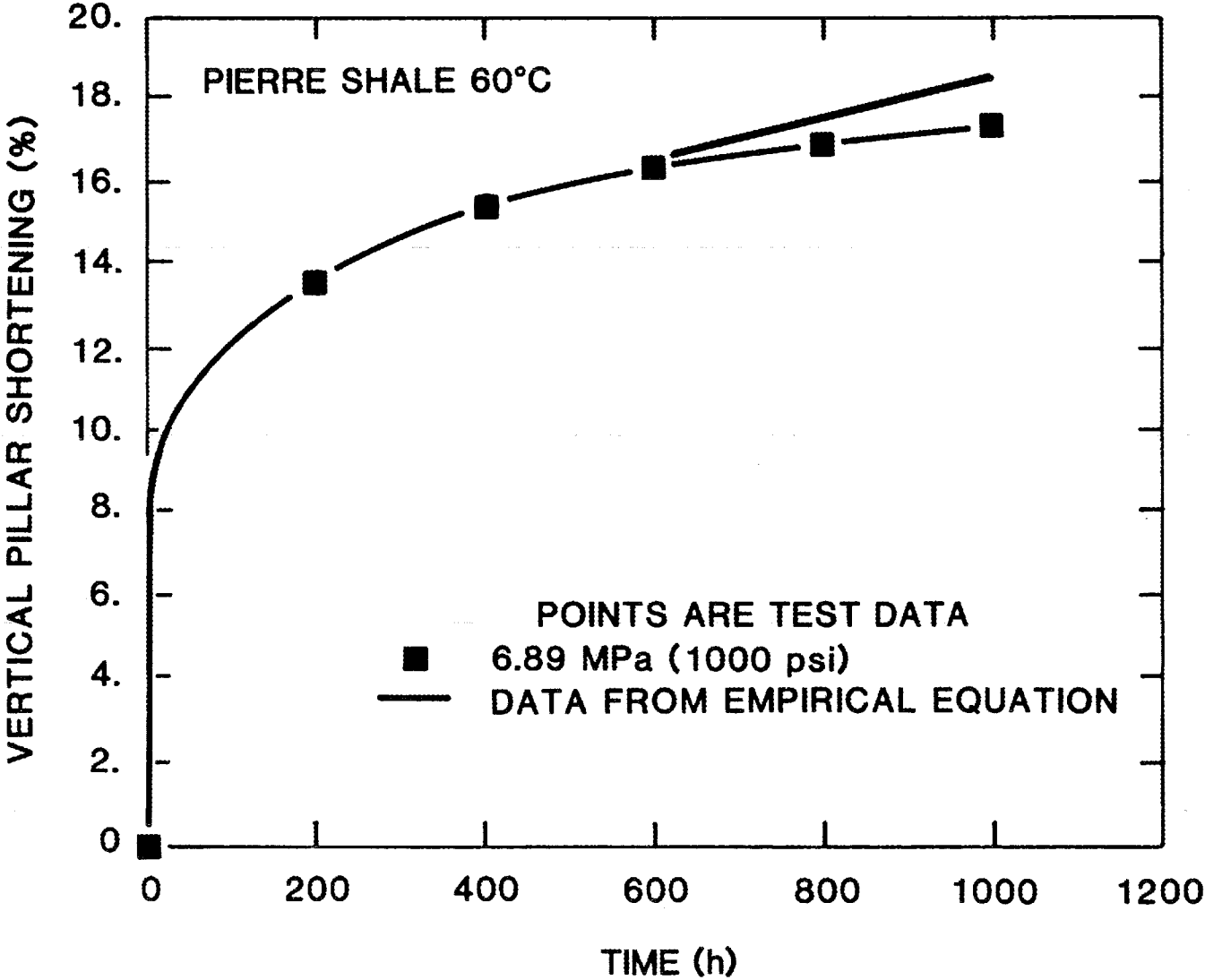


Fig. 6. Pillar shortening for Pierre Shale at 60°C.

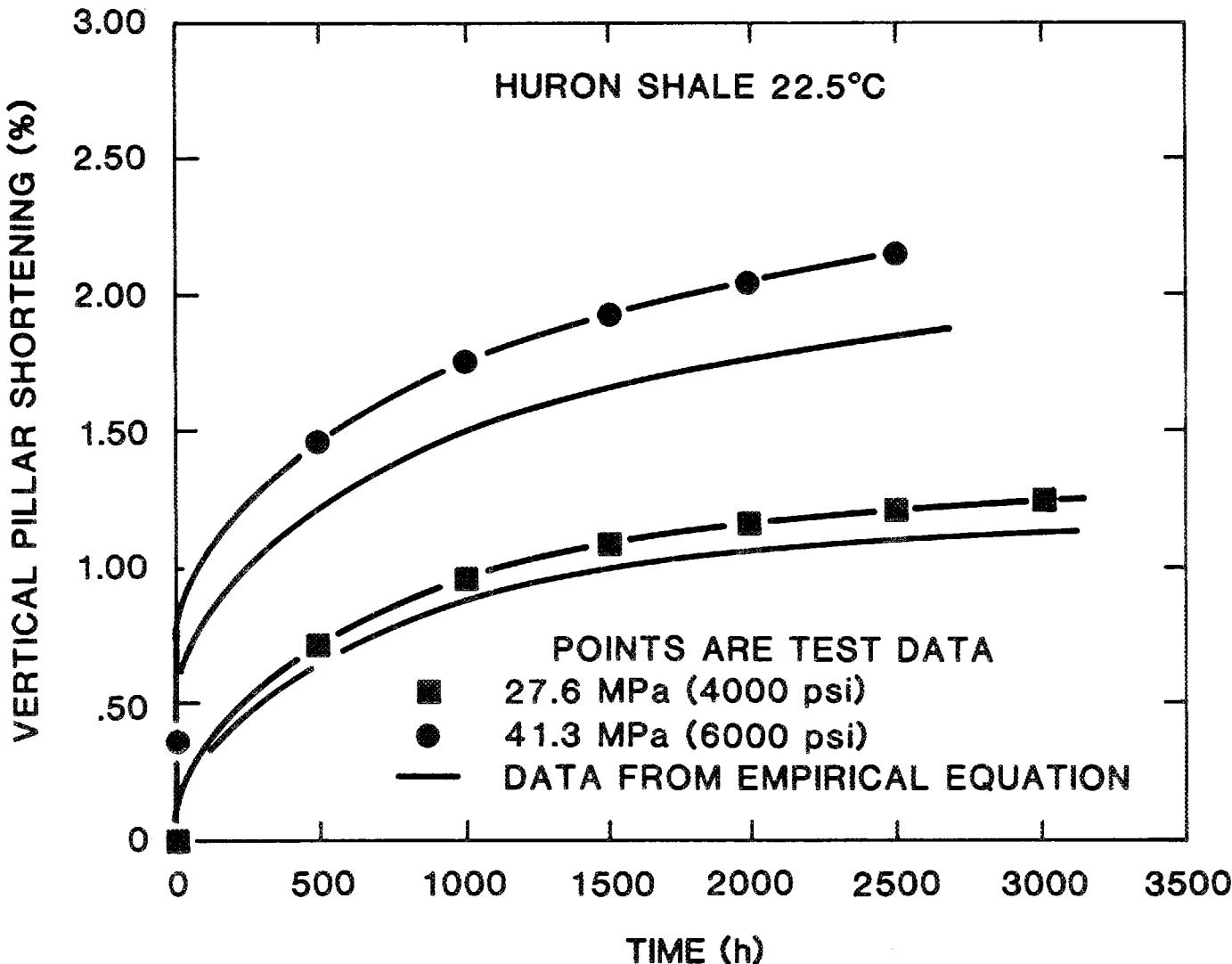


Fig. 7. Pillar shortening for Huron Shale at 27.6 MPa and 41.3 MPa.

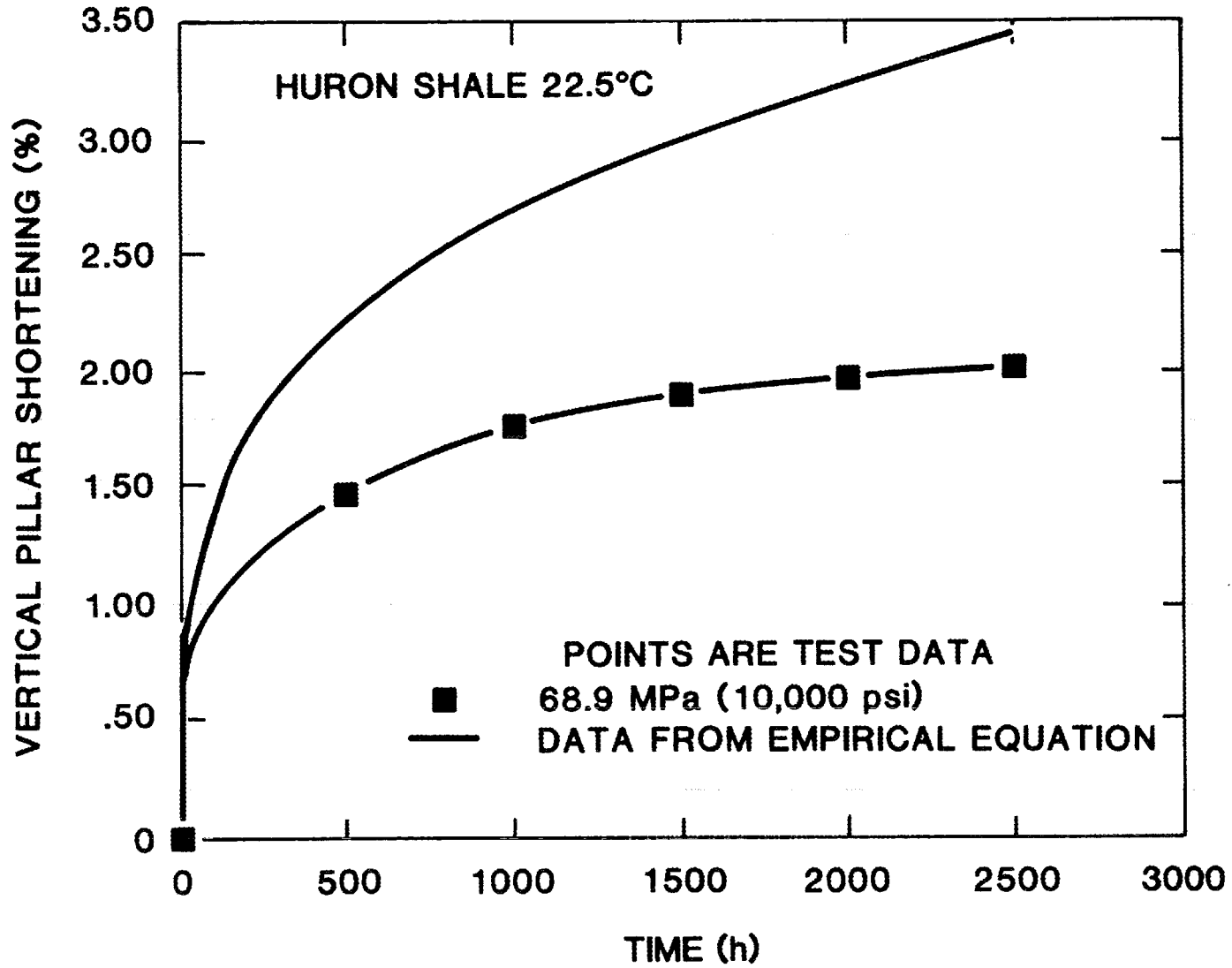


Fig. 8. Pillar shortening for Huron Shale at 22.5°C.

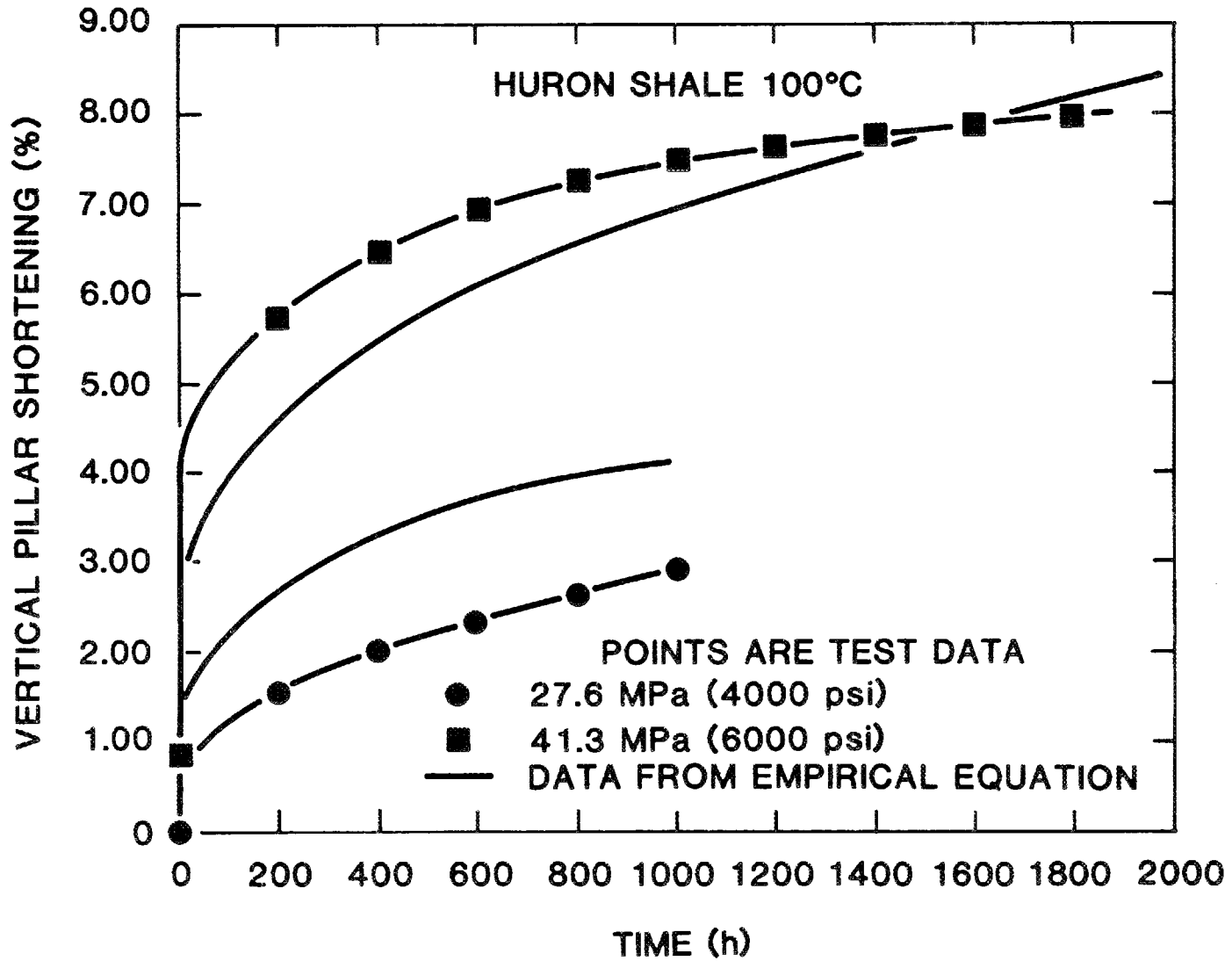


Fig. 9. Pillar shortening for Huron Shale at 100°C.

where ϵ is the fractional pillar shortening (which is dimensionless), σ is the initial average pillar stress in psi (1 MPa = 145 psi), T is the absolute temperature in K, and t is the time in hours. The parameters (A , n , u , and m) used in Eq. (3) may be found by either (1) a nonlinear curve fitting method, such as the path of steepest descent, or (2) by first linearizing the equation (by taking logarithms of both sides) and determining the parameters by multiple linear regression. Because of the scoping nature of this study, the second approach was chosen to provide preliminary values for the parameters.

The logarithm of Eq. (3) becomes

$$\log(\epsilon) = \log(A) + n \log(\sigma) + u \log(T) + m \log(t), \quad (4)$$

which is suitable for multiple linear regression.

The parameters for the model of Eq. (3) have been estimated for each of the four shales tested in this study and are shown in Table 5 along with the applicable ranges of initial stress, temperature, and time. Note that these parameters hold for the geometries given in Table 2, particularly for $W/H = 4$. Also, these parameters are limited to the shales described in Table 1. These parameters are likely to be sensitive to changes in shale composition (particularly the amounts of smectite and other clays, quartz, feldspar, and kerogen for the Green River Formation), moisture content, and porosity. In view of these limitations and the small size of the data base used, parameter values given in Table 5 must be considered very preliminary.

Note that the time range of applicability of some of the tests, as given in Table 5, is somewhat less than the duration of the corresponding tests shown in Table 3. This difference is due to irregularities in the data caused by power outages and pressure leaks.

The room temperature, 69 MPa (10,000 psi) test on the Conasauga Formation was not used in the data base because initial fractures developed on the pillar surface during loadup and because its behavior was considerably different from the remaining Conasauga tests. The room temperature test at 14 MPa (2000 psi) on the Pierre Shale also caused spalling on the pillar surface during loadup. We note that the unconfined compressive strength of the Pierre Shale from Table 1 is 7.2 MPa or about 1044 psi; therefore, it is not surprising that

Table 5. Parameters for empirical model^a

Rock type	A (psi) ⁻ⁿ (K) ^{-u} (h) ^{-m}	n	u	m	Stress range (psi) ^b	Temp. range (°C)	Time range (hr)
Green River Formation	3.2669 x 10 ^{-9c}	1.5013	0	0.23338	4000- 6000	22.5	0- 1000
Conasauga Group	2.7739 x 10 ⁻¹⁸	1.8796	3.2760	0.26878	4000- 6000	22.5- 100	0- 1000
Pierre Shale	3.4719 x 10 ⁻²⁵	1.9902	6.7885	0.20995	1000- 2000	22.5- 60	0- 1000
Huron Shale	2.2630 x 10 ⁻²⁵	1.2906	6.9335	0.26199	1000- 4000	22.5- 100	0- 3145

^a $\epsilon = a\sigma^n T^u t^m$ where ϵ is dimensionless, σ is in psi, T is in K, and t is in hours. Stress, temperature, and time ranges of applicability are given.

^b1 MPa = 145 psi.

^cFive digits are shown for the parameters in the empirical models in order to provide consistent results for shortening, because rounding of parameters may introduce inconsistencies in model results. Model values for shortening should be reported to three significant digits.

localized failures occur when the average pillar stress is 14 MPa (2000 psi). In this case, the 2000 psi test was left in the data base, and the results shown on Figs. 5 and 6 indicate that the empirical model does a relatively good job of tracking the data.

The room temperature test at 69 MPa (10,000 psi) for the Huron Shale (Fig. 8) was left in that data base, but Fig. 9 indicates that its behavior is not consistent with the other Huron Shale results. If these test data were eliminated from the data base, it is likely that the model parameters would change slightly, and the fits to the remaining data would improve. In this case, initial fractures were not reported during loadup, and we have no data on the unconfined compressive strength of the Huron Shale.

The temperature exponent given in Table 5 for the Green River Formation is zero because no data are available at elevated temperatures.

The only statistics calculated for the comparisons between the empirical model and the pillar shortening data (shown on Figs. 2 to 9) are the root mean square (RMS) differences which are given in Table 6. Note that these RMS values are relative to the magnitude of the shortening for each test and cannot be directly compared unless they are normalized by dividing by the maximum fractional shortening for each test. In general, small RMS differences imply good fits to the data.

Several general observations can be made about the response of the shale model pillars. In general, the transient response of shale model pillars is similar to that of model pillars of rock salt (Lomenick and Bradshaw, 1969 and 1986). In both cases, higher stress and/or temperature lead to higher displacement rates and more cumulative displacement. However, as can be seen from Table 5, the stress exponents for the shales tested tend to be significantly lower than those for rock salt, as shown in Eq. (1). The Pierre and Conasauga samples show the highest stress sensitivity, with exponents of about 2 and 1.9, while the Huron, with an exponent of about 1.3, shows the least stress sensitivity to shortening.

The temperature sensitivity of the Pierre and the Huron Shales are about the same with exponents of about 6.8 and 6.9, compared with exponents of about 3.3 for the Conasauga Group Shale and 9.5 for

Table 6. Root Mean Square (RMS) differences between empirical model and test data

Rock type	Stress [MPa(psi)]	Temp. (°C)	RMS difference in shortening	Approx. max. short, ϵ_{\max}	$\frac{\text{RMS}}{\epsilon_{\max}} \times 100$ (%)
Green River Formation	28(4000)	22.5	2.06×10^{-4}	4.5×10^{-3}	4.6
	41(6000)	22.5	4.13×10^{-3}	7.2×10^{-3}	5.7
Conasauga Formation	28(4000)	22.5	1.17×10^{-3}	1.0×10^{-2}	11.7
	41(6000)	22.5	2.61×10^{-3}	2.4×10^{-2}	10.9
	28(4000)	100	2.20×10^{-3}	3.4×10^{-2}	6.5
Pierre Shale	7(1000)	22.5	1.14×10^{-2}	1.0×10^{-1}	11.4
	14(2000)	25.5	3.26×10^{-2}	2.7×10^{-1}	12.1
	7(1000)	60	4.21×10^{-3}	1.7×10^{-1}	2.5
Huron Shale	28(4000)	22.5	5.50×10^{-4}	1.2×10^{-2}	4.6
	41(6000)	22.5	2.63×10^{-3}	2.2×10^{-2}	12.0
	69(10,000)	22.5	6.37×10^{-3}	2.0×10^{-2}	31.9
	41(6000)	100	8.93×10^{-3}	8.0×10^{-2}	11.2
	28(4000)	100	1.01×10^{-2}	2.8×10^{-2}	36.1

rock salt. Consequently, the temperature sensitivity of transient creep response of the shales tested was less than rock salt but is still very significant. Table 1 lists both ambient and 150°C strength data for the shales from the Green River Formation (Hansen, and Vogt, 1987). The higher temperature apparently weakens the Green River Formation Shales dramatically. Unfortunately, we have no model pillar data at elevated temperatures for the Green River Formation Shales to use for comparison.

Time exponents for the four shales show a remarkable consistency, ranging from a low of about 0.21 for the Pierre to a high of about 0.27 for the Conasauga. These values compare with a nominal value of 0.3 for rock salt. The lower value of the average time exponent for shale indicates that the creep rate for shale is likely to decrease faster than that for rock salt. In fact, for some cases, notably the Conasauga Group Shale at 22.5°C and 28 MPa (4000 psi), shown on Fig. 3, the convergence rate is about zero for the last several hundred hours of the test. A similar situation is observed for the Huron Shale at 100°C and 41 MPa (6000 psi), shown on Fig. 9, and the room temperature Huron Shale at 41 MPa (4000 psi), shown on Fig. 7. This behavior indicates that the transient creep model used in this study and previously used in the study of closure of model pillars of salt, may not be appropriate for the time dependent response of model pillars of shale. A more appropriate time function for the empirical model may be

$$1 - \exp (t/t_c), \quad (5)$$

where t_c is the time required for the pillar shortening, ϵ , to approach its final value. It is interesting to note that Stage I of the triaxial creep test reported by Hansen and Vogt (1987) (Fig. E-1, p. 79) apparently exhibits this same phenomenon, while stages II and III at higher temperature and stress difference, respectively, indicate continued straining with time. Hansen and Vogt's unconfined creep test (Fig. E-2, p. 80), however, again indicates the approach of a terminal strain at room temperature. At this time, we have no firm understanding of the microscopic creep mechanisms in these shales and, consequently, can come to no firm conclusions, especially in view of the small data base in the scoping study.

The shales tested during the scoping study may be ranked according to how much their model pillars shortened at a constant stress, temperature, and time. Pierre Shale model pillars were tested at lower stresses than the other shales, but they deformed more. Consequently, the Pierre Shale is the most easily deformed of the group tested. The remaining three shales were tested at 28 MPa (4000 psi) and 41 MPa (6000 psi), which allows direct comparison at 22.5°C and 1000 h, as shown on Table 7. Note that for the above conditions, the Conasauga Group Shale pillars deformed the most, followed closely by the Huron Shale and the Green River Formation Shale, which is much less deformable for the stated conditions.

Table 7. Comparison of approximate dimensionless pillar shortening at 22.5°C and 1000 hr for two stresses

	29 MPa (4000 psi)	41 MPa (6000 psi)
Conasauga Group Shale	0.010	0.024
Huron Shale	0.008	0.017
Green River Formation Shale	0.0046	0.0072

6. CONCLUSIONS

Based on model pillar tests of four different shales, we conclude that model pillars of these shales exhibit time dependent closure and that the rate of closure is increased by both increases in the initial pillar stress and the test temperature. The power-law transient creep equation has been used as the empirical pillar creep model for these shales, and the comparisons between empirical model results and laboratory data are reasonably good for the range (stress, temperature, and time) of applicability of the empirical model. We have compared the deformational response of the shale model pillars with that of model pillars of rock salt and found both similarities and differences: (1) salt pillars appear to be more sensitive to both

temperature and stress than shale pillars; and (2) some shale pillar data suggest that after an initial transient phase, the pillar shortening approaches a steady value. When more data become available, a quantitative comparison will be possible.

The scoping study on model pillar shortening provides preliminary information useful in investigations for a national survey of potential shales to host a nuclear waste repository. The weaker, more deformable Pierre Shale, would probably be most useful where strata of sufficient thickness occur relatively close to the surface where overburden stresses and temperatures are likely to be lower. On the other hand, repository depths for the other shale types considered, could vary over a much wider range. The scoping data are too few to set any limits at this time. For example, at 22.5°C, the Green River Formation Shale appears to be the strongest and least deformable of the shales considered herein; however, Hansen and Vogt (1987) report a decrease in strength from 94.8 MPa (13,700) psi at room temperature to 24.7 MPa (3580 psi) at 150°C.

Future work on shale should consider the role of (1) moisture content, (2) moisture loss through heating, (3) pore pressure increases caused by heating and rapid stress increases, and (4) the possible influence of pore fluid chemistry on strengths and deformations of the shales. The influence of each of these considerations is likely to vary with the clay mineral content of the shales. In particular, the smectite-rich Pierre Shale may shrink significantly when drying during a test at elevated temperature. Shrinking caused by drying would presumably add to the strain induced by the stress until most of the water has been forced out. To the author's knowledge, the above noted effects of moisture on deformation have not been systematically studied as they relate to pillars in shale.

7. REFERENCES

1. Bradshaw, R. L. and McClain, W. C. 1971. Project Salt Vault: A Demonstration of the Disposal of High Activity Solidified Wastes in Underground Salt Mines, ORNL-4555, Oak Ridge National Laboratory, 1971.
2. Gonzales, S., Johnson, K. S., and Potter, P. E. 1985. "Geologic Characteristics of Shale, Appendix E.2," Evaluation of Five Sedimentary Rocks Other than Salt for High-Level Waste Repository Siting Purposes, ORNL/CF-85/2/V2, 1985.
3. Hansen, F. D. and Vogt, T. J. 1987. Thermomechanical Properties of Selected Shales, RSI-0305, Re/Spec, Inc., June 1987.
4. Hubbert, M. K. 1937. "Theory of Scale Models as Applied to the Study of Geologic Structures," Geol. Soc. Am. Bull. 48, 1459-1520 (1937).
5. Lomenick, T. F. and Bradshaw, R. L. 1969a. "Deformation of Rock Salt in Openings Mined for the Disposal of Radioactive Wastes," Rock Mechanics 1, 5-30 (1969).
6. Lomenick, T. F. and Bradshaw, R. L. 1969b. "Model Pillar Tests for Evaluating the Structural Stability of Openings in Rock Salt Utilized for the Disposal of Radioactive Wastes," Nuclear Engineering and Design 9, 269-278 (1969).
7. Obert, L. E. 1964. "Deformational Behavior of Model Pillars Made from Salt, Trona, and Potash Ore," Proceedings of Sixth Symposium on Rock Mechanics, Rolla, MO, 539-560 (1964).
8. Obert, L. and Duvall, W. I. 1967. Rock Mechanics and the Design of Structures in Rock, John Wiley and Sons, New York (1967).
9. Russell, J. E. and Lomenick, T. F. 1984. "Analysis of Long-Term Creep Tests on Model Pillars," The Mechanical Behavior of Salt, Trans Tech Publications, Clausthal, FRG, 1984, pp. 355-368.
10. Thoms, R. L. et al. 1973. "Finite-Element Analysis of Rock-Salt Pillar Models," New Horizons in Rock Mechanics, Proceedings Fourteenth Symposium on Rock Mechanics, Pennsylvania State University, American Society Civil Engineers, 1973, pp. 363-405. (1973).
11. Wahi, K. K., et al. 1977. A Two-Dimensional Simulation of the Thermomechanical Response of Project Salt Vault, Y/OWI-Sub-77/16549/162, SAI-Oakland, prepared for Office of Waste Isolation, Union Carbide Corporation-Nuclear Division (1977).

INTERNAL DISTRIBUTION

1. A. G. Croff
2. R. B. Dreier
3. T. W. Hodge, Jr.
4. O. C. Kopp
- 5-9. T. F. Lomenick
10. T. H. Row
11. S. H. Stow
12. V. C. A. Vaughen
13. R. G. Wymer
- 14-15. Central Research Library
- 16-17. Laboratory Records
18. Laboratory Records -- RC
19. ORNL Patent Section
20. ORNL Y-12 Technical Library, Document Reference Section

EXTERNAL DISTRIBUTION

21. Office of Assistant Manager for Energy Research and Development, Department of Energy, Civilian Radioactive Waste Management, 1000 Independence Ave., Washington, DC 20545
22. C. R. Cooley, Department of Energy, 1000 Independence Ave., Washington, DC 20545
23. S. H. Kale, Department of Energy, 1000 Independence Ave., Washington, DC 20545
24. R. C. Baker, Department of Energy, Chicago Operations Office, 9800 S. Cass Ave., Chicago, IL 60439
25. S. Mann, Department of Energy, Chicago Operations Office, 9800 S. Cass Ave., Chicago, IL 60439
26. J. D. Kasprowicz, Department of Energy, Chicago Operations Office, 9800 S. Cass Ave., Chicago, IL 60439
27. Office of Assistant Manager for Energy Research and Development, DOE-ORO, P. O. Box E, Oak Ridge, TN 37831
28. Neil Chapman, Institute of Geological Sciences, Exhibition Road, South Kensington, UK-London, SW72DE, United Kingdom
29. D. Gray, Institute of Geological Sciences, Exhibition Road, South Kensington, UK-London, SW72DE, United Kingdom
30. R. Heremans, National Agency for Radioactive Waste and Fissile Materials Mgt. ONDRAF/NIRAS, Boulevard du Regent 54-Boite 5, 1000 Brussels, Belgium
31. P. Manfroy, National Agency for Radioactive Waste and Fissile Materials Mgt. ONDRAF/NIRAS, Boulevard du Regent 54-Boite 5, 1000 Brussels, Belgium
- 32-34. W. E. Newcomb, Office of Waste Technology, Battelle Project Management Division, 7000 S. Adams St., Willowbrook, IL 60521
35. A. K. Yonk, Office of Waste Technology, Battelle Project Management Division, 7000 S. Adams St., Willowbrook, IL 60521

36. A. Fossom, RE/SPEC, Inc., P. O. Box 725, Rapid City, SD 57701
37. P. F. Gnirk, RE/SPEC, Inc., P. O. Box 725, Rapid City, SD 57701
38. F. D. Hansen, RE/SPEC, Inc., P. O. Box 725, Rapid City, SD 57701
39. M. Loken, RE/SPEC, Inc., P. O. Box 725, Rapid City, SD 57701
40. J. L. Ratigan, RE/SPEC, Inc., P. O. Box 725, Rapid City, SD 57701
41. T. J. Vogt, RE/SPEC, Inc., P. O. Box 725, Rapid City, SD 57701
42. N. L. Carter, Petroleum Engineering and Geophysics, Texas A&M University, College Station, TX 77843
43. P. A. Domenico, Petroleum Engineering and Geophysics, Texas A&M University, College Station, TX 77843
44. J. E. Russell, Petroleum Engineering and Geophysics, Texas A&M University, College Station, TX 77843
45. W. C. McClain, Roy F. Weston, Inc., 2301 Research Boulevard, Rockville, MD 20850
46. S. Panno, Roy F. Weston, Inc., 2301 Research Boulevard, Rockville, MD 20850
47. P. E. Ahlstrom, SKBF, Box 5864, S-102 48 Stockholm, Sweden
48. A. Barbreau, Commissariat a l'Energie Atomique, Inst de Protection et de Surete Nucleaire, Centre d'Etudes Nucleaires, B. P. No. 6, F-92260, Fontenay-Aux-Roses, France
49. Z. T. Bieniawski, Penn State University, University Park, PA 16802
50. A. Bonne, Belgian Nuclear Research Center, CEN/SCK, Boeretang 200, B.2400 Mol, Belgium
51. P. J. Bourke, UKAEA, B-151, Chem. Tech. Division, Atomic Energy Research Establishment, Harwell, GB-OXON, ORA, United Kingdom
52. W. Brewitz, Gesellschaft fur Strahlen und Umweltforschung mbH Munchen, Institut fur Tieflagerung, Wissenschaftliche Abteilung, Theodor-Heussstrasse 4, D-3300 Braunschweig, FRG
53. D. Caldwell, Golder Associates, 2950 North Up Way, Bellevue, WA 98004
54. J. A. Cherry, Dept. of Earth Sciences, University of Waterloo, Waterloo, Ontario, Canada, N2L 3G1
55. J. O. Duguid, ICP Technology, 1850 K Street, N.W., Washington, DC 20006
56. Ferruccio Gera, Ismes Spa, 24100 Bergamo-Viale G. Cesare 29, Taramelli 14, 00197 Rome, Italy
57. S. Gonzales, Earth Resource Associates, Inc., 295 East Dougherty Street, Suite 105, Athens, GA 30601
58. J. Handin, 2614 Melba Circle, Bryan, TX 77892
59. D. Hansen, 2810-130 PL NE, Bellevue, WA 98005
60. M. P. Hardy, Agapito Associates, Inc., Suite 340, 715 Horizon Drive, Grand Junction, CO 81505
61. B. Y. Kanehiro, Berkeley Hydrotechnique, Inc., 2150 Shattuck Ave., Berkeley, CA 94704

62. K. Kuhn, Head of Institute, GSF, Berliner Strasse 2, D-3392 Clausthal-Zellerfeld, FRG
63. A. R. Lappin, Sandia National Laboratories, P. O. Box 5800, Albuquerque, NM 87185
64. W. G. Pariseau, University of Utah, Salt Lake City, UT 84112
65. Frank L. Parker, Vanderbilt University, Nashville, TN 37203
66. T. Pigford, Dept. of Nuclear Engineering, College of Engineering, University of California, Berkeley, CA 94720
67. P. E. Potter, Department of Geology, University of Cincinnati, Cincinnati, OH 45221
68. Atou Shimosato, Nuclear Power Generation Division, Hitachi, Ltd., 6 Kanda-Surugadai 4 Chome, Chiyoda-Ku, Tokyo 01, Japan
69. H. W. Smedes, 1126 Buehler Dr., Las Vegas, NV 89102
70. P. R. Stevens, Department of the Interior, U.S. Geological Survey, Reston, VA 22092
71. H. S. Swolfs, Department of the Interior, U.S. Geological Survey, Federal Center, Denver, CO 80225
72. K. T. Thomas, Waste Management Section, Division of Nuclear Fuel Cycle, International Atomic Energy Agency, Wagramerstrasse 5, P. O. Box 200, A-1400 Vienna, Austria
73. M. F. Thury, NAGRA-National Cooperative for the Storage of Radioactive Waste, Parkstrasse 23, CH-5401 Baden, Switzerland
74. W. S. Twenhofel, 820 Estes Street, Lakewood, CO 80215
75. P. Venet, Commission of the European Communities, Directorate General XII, Nuclear Fuel Cycle Division, 200 Rue de la Loi, B-1040 Brussels, Belgium
76. S. H. Whitaker, Applied Geoscience Branch, Atomic Energy of Canada, Ltd., Whiteshell Nuclear Research Establishment, Pinawa, Manitoba ROE 1 LO, Canada
- 77-106. Technical Information Center, Oak Ridge, TN 37830

